Elastic FWI with rock physics constraints

Qi Hu and Kris Innanen

ABSTRACT

Current efforts to use elastic full waveform inversion (EFWI) go beyond imaging of complex structures and aim at determination of reservoir-scale rock physics properties. However, the nonlinearity of EFWI and parameter crosstalk can prevent its convergence toward the actual model. Parameters such as density and fluid saturation are more difficult to retrieve because of their limited contributions to seismic data. We develop a method for EFWI that uses rock physics constraints to mitigate such limited sensitivity. These constraints are in the form of explicit velocity-density relations for different lithologic facies as a function of position, and are imposed through a model regularization term in the objective function. We implement two different workflows of constraining EFWI for elastic and rock physics properties. One is a sequential approach that consists of first inverting for velocity and density through EFWI and then transforming the elastic attributes to rock physics properties. The other is a joint approach where we parameterize EFWI with rock physics properties, allowing elastic and rock physics properties to be simultaneously updated. Constraining each workflow helps improve density and saturation recoveries. We also illustrate that the joint approach is superior to the sequential inversion in terms of computational cost and the ability to ensure consistency between elastic and rock physics properties.

INTRODUCTION

Elastic full waveform inversion (EFWI) is concerned with the simultaneous determination of two or more subsurface elastic properties. Despite the increasing implementation of EFWI in properly imaging and interpreting the subsurface, several key challenges remain. For instance, EFWI is a highly nonlinear and ill-posed problem, so the model updates are often trapped in local minima (Bunks et al., 1995; Operto et al., 2013; Geng et al., 2018; Pan et al., 2018). Moreover, EFWI suffers from parameter crosstalk, which arises from the complex manner in which multiple elastic properties co-determine seismic waveforms, and occurs when errors in one parameter are mapped into the updates of another (Métivier et al., 2017; Pan et al., 2018, 2019; Keating and Innanen, 2019).These issues increase the uncertainty of the inverse problem and could lead to subsurface model that does not represent realistic lithology (Aragao and Sava, 2020).

Regularization techniques allow to stabilize ill-posed inverse problems by incorporating prior information about the model in the inversion. Prior information can consist of estimates of model parameters (Asnaashari et al., 2013) or expected structure of the model, e.g., smoothness (Tikhonov and Arsenin, 1977) or blockiness (Guitton, 2012). In recent years, some authors propose using physical relationships between elastic parameters as prior information to constrain the inversion. Because these relationships vary with lithofacies and are commonly derived from well logs, the corresponding model constraint is often called facies-based rock physics constraint (Kamath et al., 2017; Singh et al., 2018; Zhang et al., 2018) or petrophysical constraint (Rocha and Sava, 2018; Aragao and Sava, 2020). Their methods distinguish with each other by the form of mode penalty term included in

the objective function. For example, Rocha and Sava (2018) use a logarithmic function to confine the inverted models to a region defined by linear trends between model parameters. Aragao and Sava (2020) propose using probability density functions to impose complex petrophysical relations. Zhang et al. (2018) use a facies-based prior model term and update it iteratively during the inversion. These approaches have been demonstrated to guide the inversion toward high-resolution and geologically plausible elastic models.

Most efforts to involve EFWI in rock physics model reconstruction are of a sequential type, that is, the elastic attributes are first inverted from seismic data via EFWI, and they are next transformed to rock physics properties, such as porosity, lithology, and fluid saturation (Grana, 2016; Dupuy et al., 2016a,b). Therefore, if constraining EFWI helps improve elastic models, it should also lead to more accurate reconstructions of rock physics properties. As opposed to the sequential approach, Hu et al. (2020) propose formulating EFWI with rock physics model parameterizations. Because they unify EFWI and rock physics in a single formulation, their approach accounts for the elastic and rock physics properties together, allowing them to be jointly updated. Their results illustrate that parameter crosstalk is generally an issue for recovering rock physics properties, and water saturation is most challenging to estimate due to its minor contribution to seismic data. This raises the question of whether the regularization techniques designed to improve elastic models can be incorporated into the joint approach for a better estimation of rock physics properties.

In this study, we propose a model penalty term based on explicit relations between velocity and density. We assume that the relations are facies-dependent, and can be obtained, for example, by fitting well-log data. We first discuss general aspects of EFWI, emphasizing the mechanisms used to incorporate this constraint. Then, we use a simple synthetic model, which contains only one facies, to test both the sequential and joint workflows for recovering elastic and rock physics properties. For each workflow, we show the improvement obtained by imposing the model constraint. We also illustrate some favorable features of the jointly inverted models. Finally, on a selected target of the Marmousi model, we demonstrate the potential and challenges of applying the proposed method to multi-facies cases.

THEORY

EFWI with model constraint

The general definition of the objective function for solving ill-posed inverse problems could be recast as the Tikhonov function (Tikhonov and Arsenin, 1977; Asnaashari et al., 2013):

$$E(\mathbf{m}) = E_d(\mathbf{m}) + \lambda E_m(\mathbf{m}), \tag{1}$$

where the data misfit term $E_d(\mathbf{m})$ is based on a norm of the residuals between observed data $\mathbf{d}_{obs}$ and synthetic data $\mathbf{d}(\mathbf{m})$ simulated from model $\mathbf{m}$, and the model term $E_m(\mathbf{m})$ is based on a norm of a model penalty function. λ is the trade-off parameter that controls the relative importance of data and model term. Using the l_2 norm, $E_d(\mathbf{m})$ can be written as

$$E_d(\mathbf{m}) = \|\mathbf{W}_d(\mathbf{d}_{obs} - \mathbf{d}(\mathbf{m}))\|_2^2 = \frac{1}{2}[(\mathbf{d}_{obs} - \mathbf{d}(\mathbf{m}))^T \mathbf{W}_d^T \mathbf{W}_d(\mathbf{d}_{obs} - \mathbf{d}(\mathbf{m}))], \tag{2}$$

where $\mathbf{W}_d$ is a weighting operator on the data, and the superscript ^{T} denotes the transpose. In our study, $\mathbf{W}_d$ is chosen as identity matrix.

To impose petrophysical relations to constrain the inversion, we define the model penalty term as

$$E_m = \frac{1}{2}\sum_{\mathbf{x}}(m_1 - f(m_2))^2, \tag{3}$$

where $\mathbf{x}$ denotes model space coordinates, $m_1 = m_1(\mathbf{x})$ and $m_2 = m_2(\mathbf{x})$ are two different physical parameters, and $f = f(\mathbf{x})$ is a position-dependent function mapping m_2 to m_1. We consider an EFWI model parameterization of P-wave velocity, S-wave velocity, and density ($V_\mathrm{P}, V_\mathrm{S}, \rho$). Let m_1 represent density and m_2 represent P-wave velocity, equation 3 becomes

$$E_m = \frac{1}{2}\sum_{\mathbf{x}}(\rho - f(V_\mathrm{P}))^2. \tag{4}$$

The model term E_m forces the inverted velocity and density models to satisfy the relation $\rho = f(V_\mathrm{P})$. In general, different lithologies are subject to different velocity-density relations (e.g., Gardner et al., 1974; Castagna et al., 1993; Martin et al., 2006). We make the function $\rho = f(V_\mathrm{P})$ position-dependent so that each model cell, based on its associated lithology or geologic facies, is subject to a specific velocity-density trend. (e.g., Gardner et al., 1974; Castagna et al., 1993; Martin et al., 2006). We also assume that well logs of the two properties are available, and from which we can fit a per-facies relation between them.

Within a Newton optimization, the model vector is updated by minimizing a quadratic approximation of the objective function $E(\mathbf{m})$. The search direction $\delta\mathbf{m}$ is the solution of

$$\mathbf{H}\,\delta\mathbf{m} = -\mathbf{g}, \tag{5}$$

and

$$\mathbf{g} = \mathbf{g}_d + \lambda\mathbf{g}_m, \quad \mathbf{H} = \mathbf{H}_d + \lambda\mathbf{H}_m, \tag{6}$$

where $\mathbf{g}$, $\mathbf{g}_d$, and $\mathbf{g}_m$ are the gradients of the objective function $\mathbf{E}(\mathbf{m})$, the data misfit term $\mathbf{E}_d(\mathbf{m})$, and the model term $\mathbf{E}_m(\mathbf{m})$, respectively. $\mathbf{H}$, $\mathbf{H}_d$, and $\mathbf{H}_m$ are the corresponding Hessian operators.

In this study we use the 2D frequency-domain isotropic-elastic wave equations (Pratt, 1990), the gradient of the data misfit term with respect the model parameter m is given by (Brossier et al., 2009)

$$g_d = \Re\left\{\mathbf{u}^T\left(\frac{\partial\mathbf{A}}{\partial m_i}\right)^T(\mathbf{A}^{-1})^T\Delta\mathbf{d}^*\right\}. \tag{7}$$

where $\Re$ takes the real part of its argument, u is the incident wavefield, $\mathbf{A}$ is the impedance matrix containing frequency and medium properties, $\Delta\mathbf{d} = \mathbf{d}_{obs} - \mathbf{d}(\mathbf{m})$, and the superscript * denotes the complex conjugate.

The gradient of the model term with respect m is

$$g_m = (\rho - f(V_\mathrm{P}))\frac{\partial(\rho - f(V_\mathrm{P}))}{\partial m}. \tag{8}$$

To avoid explicitly constructing the Hessian operator $\mathbf{H}_d$, we employ a truncated Gauss Newton (TGN) method (Métivier et al., 2017), in which equation 5 is solved iteratively, involving only Hessian-vector products, which can be efficiently calculated using the adjoint state method (Plessix, 2006).

EFWI parameterized by rock physics properties

A wide range of sets of isotropic-elastic parameter classes, for instance the Lamé constants plus density, (λ, μ, ρ), or alternatively the P-wave and S-wave velocities plus density, $(V_{\mathrm{P}}, V_{\mathrm{S}}, \rho)$, can be selected for inversion (e.g., Tarantola, 1986). Although any triplet (λ, μ, ρ) can be uniquely computed from its associated triplet $(V_{\mathrm{P}}, V_{\mathrm{S}}, \rho)$, and vice versa, which is suggestive that the parameterization is irrelevant, in practice the class chosen for updating is very important.

Let $\mathbf{p} = [p_1, p_2, p_3]^T$ represent a reference EFWI parameterization, with p_i being the ith parameter class with $i = (1, 2, 3)$, so that, in the velocity/density parameterization above, for instance, p_2 represents the S-wave velocity. Let $m_i^{p_j}$ represent the model parameter in class p_j at the ith spatial position. From equation 5 we observe that this model parameter is altered at each iteration by an update proportional to $\partial \mathbf{A}/m_i^{p_j}$. To transform to a new parameterization, say $\mathbf{q} = [q_1, q_2, q_3]^T$, we compute

$$\frac{\partial \mathbf{A}}{\partial m_i^{q_j}} = \frac{\partial \mathbf{A}}{\partial m_i^{p_1}} \frac{\partial m_i^{p_1}}{\partial m_i^{q_j}} + \frac{\partial \mathbf{A}}{\partial m_i^{p_2}} \frac{\partial m_i^{p_2}}{\partial m_i^{q_j}} + \frac{\partial \mathbf{A}}{\partial m_i^{p_3}} \frac{\partial m_i^{p_3}}{\partial m_i^{q_j}}, \tag{9}$$

for each of $j = (1, 2, 3)$. Given an EFWI scheme set up to update parameters $\mathbf{p}$, within which the partial derivatives of $\mathbf{A}$ are known, and given relations between these parameters and any new desired set $\mathbf{q}$, of the form $m_i^{p_j}(m_i^{q_1}, m_i^{q_2}, m_i^{q_3})$, through equation 7 we can move to a new scheme in which the $\mathbf{q}$ are updated. This allows us to transform between different elastic parameter sets, e.g., $(V_{\mathrm{P}}, V_{\mathrm{S}}, \rho)$, (λ, μ, ρ), (κ, μ, ρ), etc.; however, it also allows us to transform from a base elastic parameter scheme to any desired petrophysical model, provided a suitable mapping exists between the parameters of this model and the three base elastic properties.

Here we consider a rock physics property model, in which $\mathbf{q}$ embodies porosity (P), clay content (C), and water saturation (Sw). The base elastic parameterization is based on P- and S-wave velocities and density. We link the two parameter sets through a representative rock physics relation: the KT model (Kuster and Toksöz, 1974), which provides V_{P}, V_{S} and ρ as explicit functions of P, C, and Sw. These relations can be used as discussed above to obtain the partial derivatives of the objective function with respect to P, C, and Sw. As a result, we formulate EFWI with a model parameterization based on the three rock physics properties, allowing them to be directly updated. Also, because the computation of V_{P}, V_{S} and ρ from P, C, and Sw is included in the EFWI forward problem, these elastic attributes are jointly updated during the inversion.

For the P-C-Sw parameterized EFWI problem, we can still deploy the model constraint

in the form of $V_{\rm P}$-ρ relations. We achieve this by rewriting Equation 4 as

$$E_m = \frac{1}{2}\sum_{\mathbf{x}}[\rho(\mathbf{m}) - f(V_{\rm P}(\mathbf{m}))]^2. \tag{10}$$

where $\mathbf{m} = (P, C, Sw)$. In other words, we constrain the inverted rock physics property model based on its elastic response.

NUMERICAL EXAMPLES

Single-facies example

In the "Theory" section we proposed adding a model penalty term in the form of $V_{\rm P}$-ρ relations to the objective function. We illustrated how this term works to constrain the EFWI that is either classically parameterized by $V_{\rm P}$-$V_{\rm S}$-ρ or parameterized by rock physics properties: P-C-Sw. The two model parameterizations correspond to two different workflows of using EFWI for elastic and rock physics properties: sequential and joint. Here we test both workflows on a single-facies synthetic model, and for each workflow we compare the proposed method with the unconstrained inversion. This leads to solving the same problem using four different approaches: unconstrained sequential inversion, constrained sequential inversion, unconstrained joint inversion, and constrained joint inversion.

We also note that within the sequential approach, the estimation of rock physics properties from the EFWI-derived elastic attributes is a nonlinear inverse problem, which is not trial to solve. We use a grid-search method (Sen and Stoffa, 2013) that involves the systematic search through each point in a predefined model space to locate the best-fit models. We make the search step small enough to ensure a precise conversion, so that no theoretical uncertainty would be brought to the converted models.

Figure 1 shows the three-layer model to recover, including its elastic properties: $V_{\rm P}$, $V_{\rm S}$, ρ and two rock physics properties: P and Sw. We create a favorable scenario by assuming a stable lithology (i.e., a single facies) and constant C (not shown). The KT model is used to relate P, Sw to $V_{\rm P}$, $V_{\rm S}$, ρ and is assumed known. Figure 2 shows the initial models, which are smoothed versions of the true models. In Figure 3 we project the true and initial models onto a $V_{\rm P}$-ρ crossplot and a P-Sw crossplot.

Figures 4 shows the recovered models using the unconstrained sequential approach. The $V_{\rm P}$, $V_{\rm S}$, and ρ models are first recovered using EFWI, they are next transformed to P and Sw models using grid search. Apart from some mild oscillatory behavior, the inverted velocity models match closely with the true models. The density model has its structure recovered, but the values of its top and middle layers overestimated to some extent. The converted porosity model is reasonably accurate, but the water saturation model is strongly distorted. Figure 5 shows the vertical profiles of the true and inverted models at a lateral position x=0.12km. We observe among the three elastic parameters a relatively large deviation of density estimate from the true model, and the deviation gets significantly more pronounced in the Sw estimate. The inverted porosity, on the other hand, matches closely the true model. Same conclusions can be drawn from the crossplots in Figure 6, which clearly demonstrate the lack of converge in Sw. Our explanation is that velocities and den-

sity are much more sensitive to porosity than to Sw, making porosity well-constrained in the conversion. Therefore even though there are obvious errors in density, porosity can be suitably recovered by the good velocity estimate. By contrast, the errors in either velocity or density become magnified in Sw.

In Figures 7, 8, and 9 the inversion results of the constrained sequential approach are summarized. The V_{P}-ρ relation used to constrain the inversion is derived by fitting the exact V_{P} and ρ data, which are assumed to be collected from well logs, with a quadratic function in the form of $\rho = aV_{\mathrm{P}}^2 + bV_{\mathrm{P}} + c$, where a, b, and c are coefficients. The fitting curve is denoted by the yellow line in Figure 9a. Imposing the model constraint confines the inverted V_{P} and ρ samples to this line. On the other hand, iteratively reducing data misfit drives these samples towards their true values. As a result, compared to the unconstrained approach, the inverted density model matches more closely the true model, which also leads to a significant improvement in Sw recovery.

We next proceed the test using the joint inversion. Unlike the sequential approach, in which rock physics is included as a cascaded step after EFWI, the joint approach accounts for the elastic and rock physics properties in a single EFWI formulation, allowing them to be simultaneously updated. In Figures 10, 11, and 12 we summarized the inversion results of the unconstrained joint approach. We observe that Sw is updated insufficiently. This is explained by Hu et al. (2020) through radiation pattern analysis, which shows very low relative scattering amplitudes from Sw. However, we note that the difficulty associated with recovering Sw here is of a different type to the sequential approach. In the latter case, the limited sensitivity of velocity and density to Sw makes the inversion of Sw unstable; in the joint approach, the very low sensitivity of seismic data to Sw makes it difficult for EFWI to produce sufficient update for this property. We also observe in Figure 11 an improved recovery of velocity and density models compared to the unconstrained sequential approach (Figure 5). This likely originates from a reduced degree of parameter crosstalk introduced by the P-Sw model parameterization.

The recovered models using the constrained joint inversion are demonstrated in Figures 13, 14, and 15. Compared to the unconstrained joint approach, the improvement to the Sw recovery is obvious: the middle layer is accurately recovered, and the spatial extent of each layer can be clearly identified. The density recovery is also slightly improved. Compared to the constrained sequential inversion, the directly estimated Sw is more stable in each layer and is free of undesired perturbations that mimic anomalies (Figure 7e). While the error magnification associated with rock physics inversion is generally an issue for the sequential approach, it is avoided in the joint inversion. This enables the latter to guarantee the consistency between elastic and rock physics property models. Moreover, by combining rock physics and EFWI in a single formulation, the joint approach avoids numerically solving the nonlinear rock physics inverse problem, therefore it is computationally more efficient.

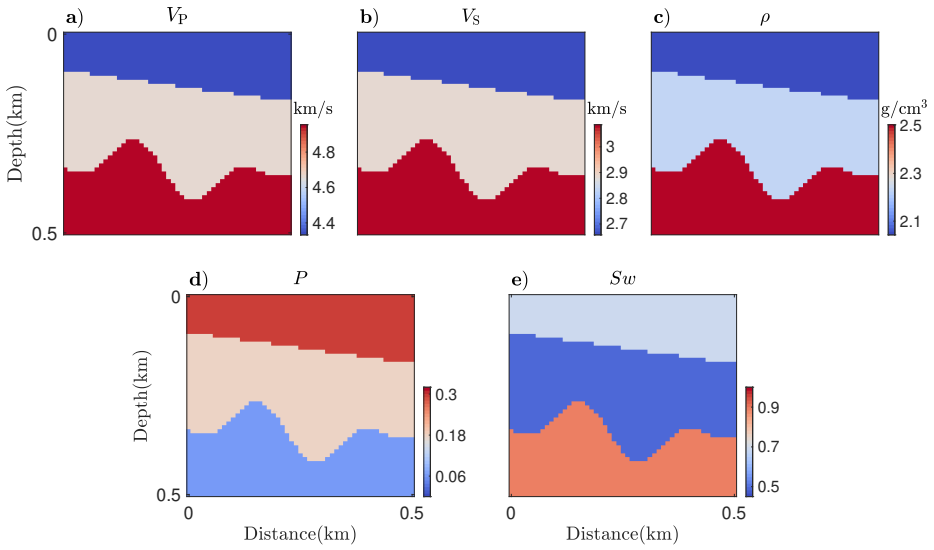

FIG. 1. True models of a) P-wave velocity, b) S-wave velocity, c) density, d) porosity, and e) water saturation. Each layer is homogeneous.

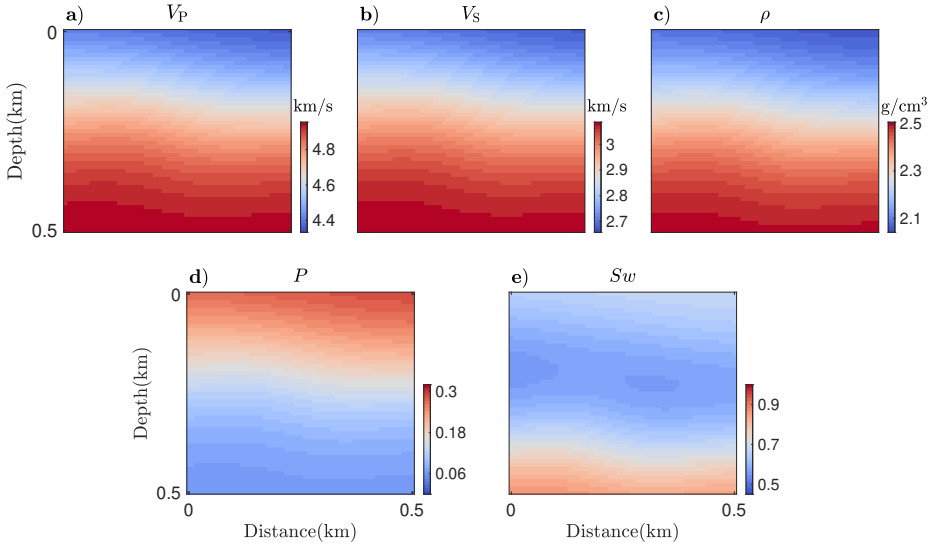

FIG. 2. Initial models. They are smoothed versions of the true models.

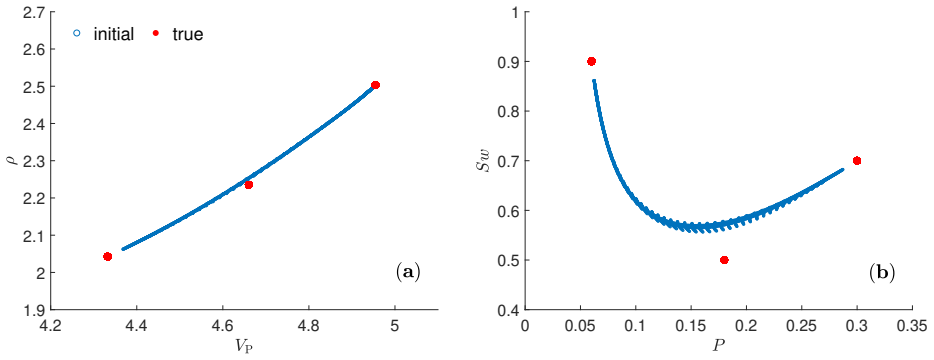

FIG. 3. True and initial models displayed in a) P-wave velocity-density crossplot, and b) porosity-water saturation crossplot.

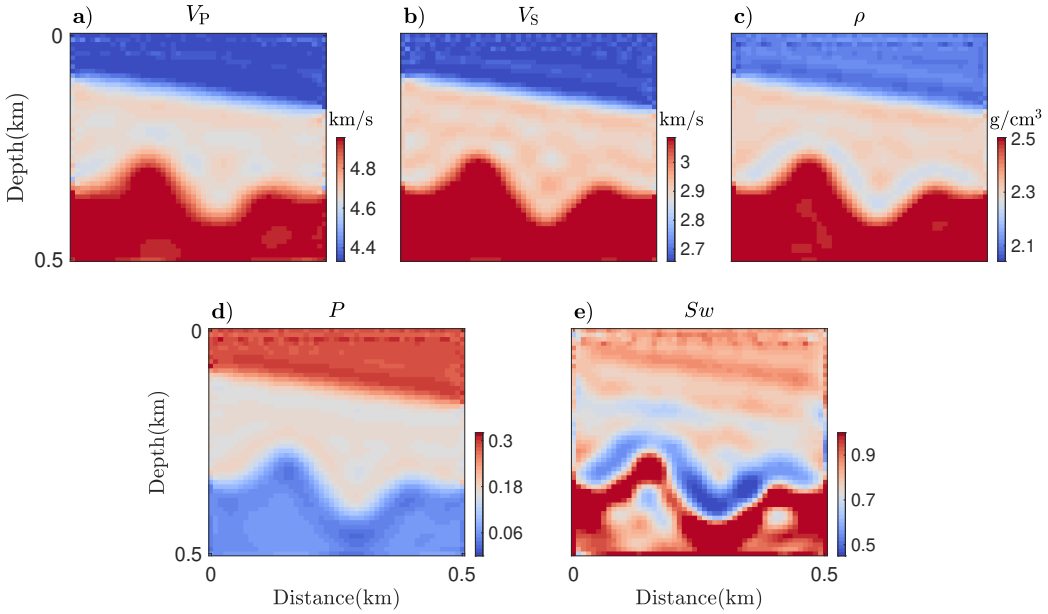

FIG. 4. Unconstrained sequential inversion: recovered models.

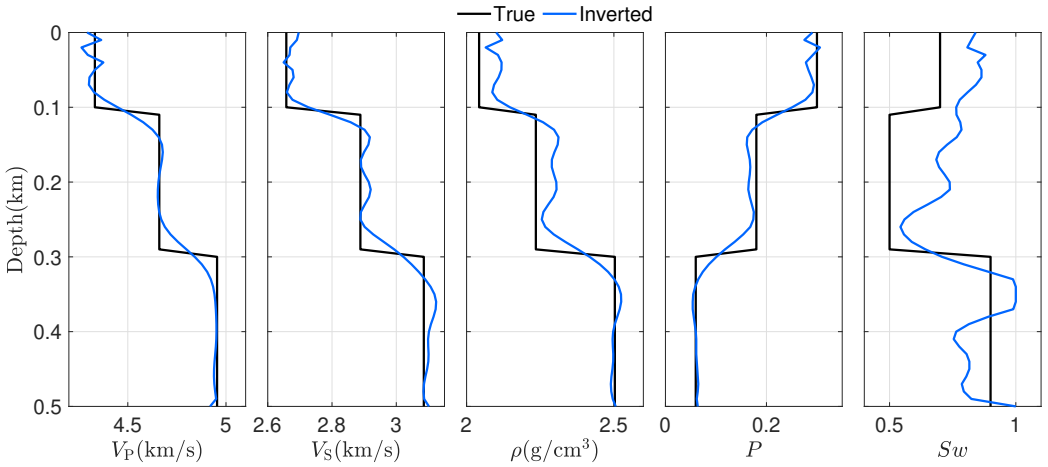

FIG. 5. Unconstrained sequential inversion: model profiles at x=0.12km.

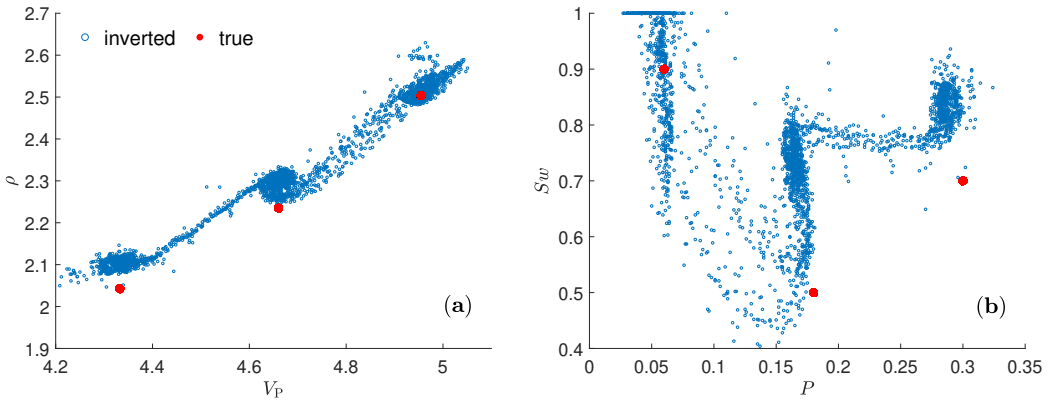

FIG. 6. Unconstrained sequential inversion: crossplots.

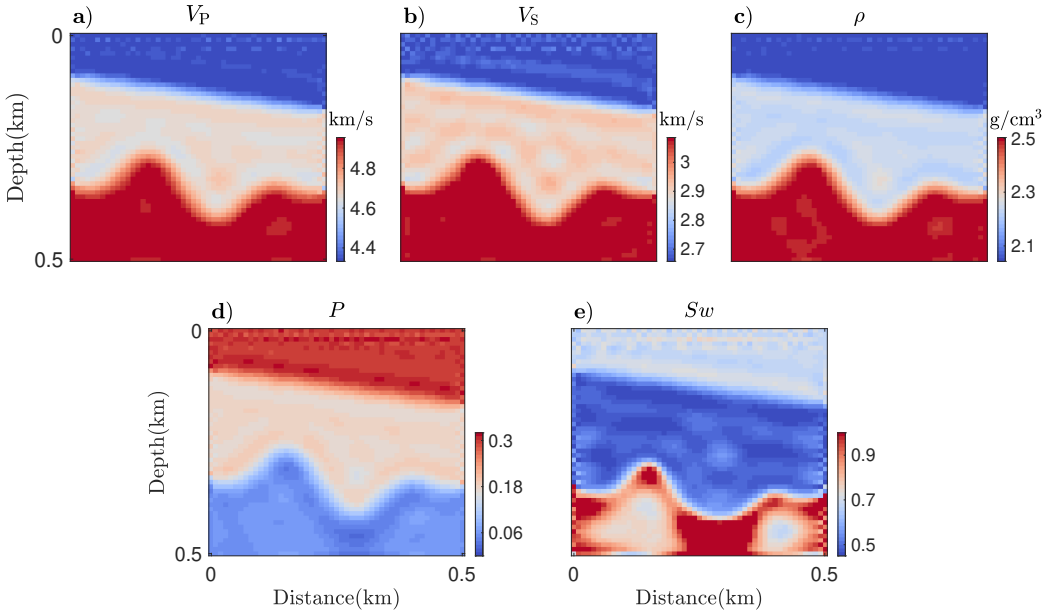

FIG. 7. Constrained sequential inversion: recovered models.

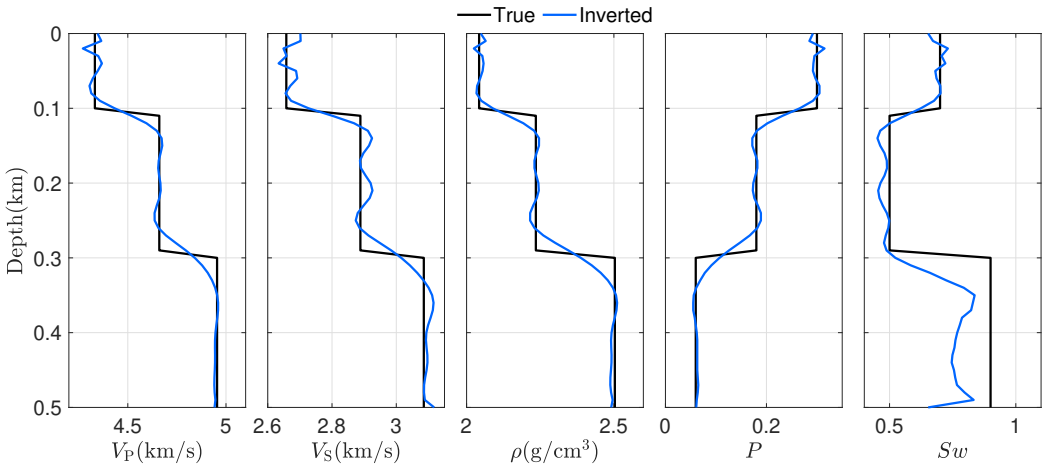

FIG. 8. Constrained sequential inversion: model profiles at x=0.12km.

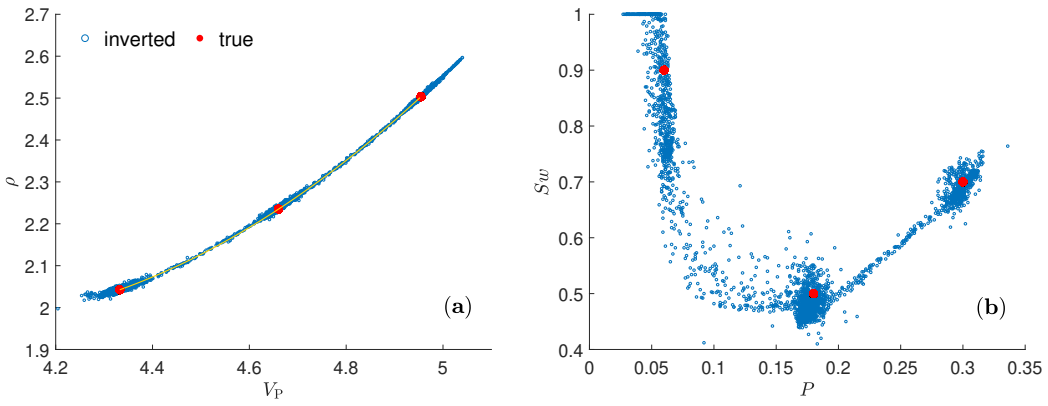

FIG. 9. Constrained sequential inversion: crossplots. The yellow line denotes the V_P-ρ relation used as constraint.

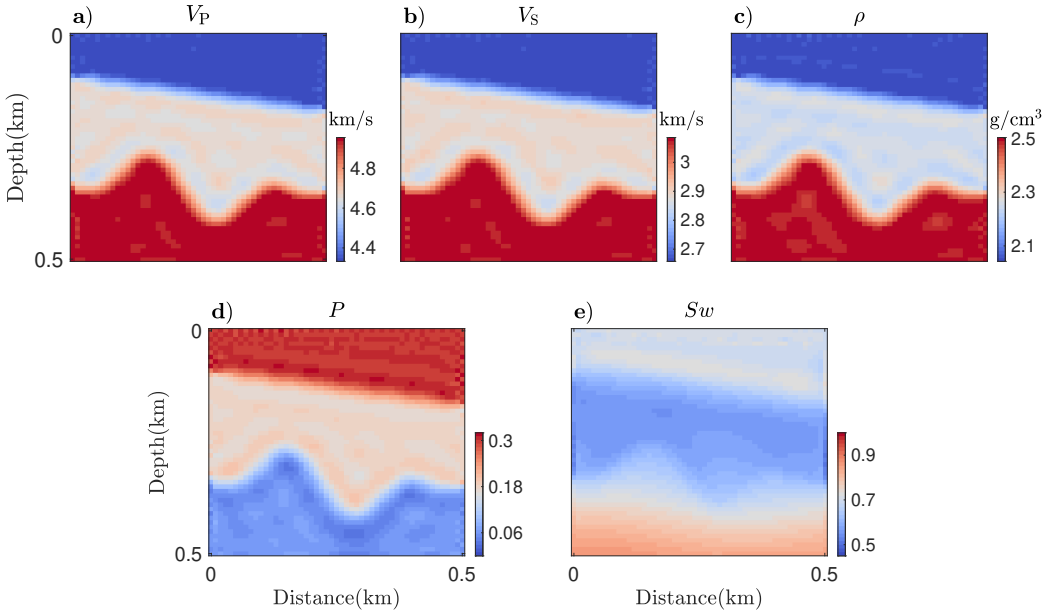

FIG. 10. Unconstrained joint inversion: recovered models.

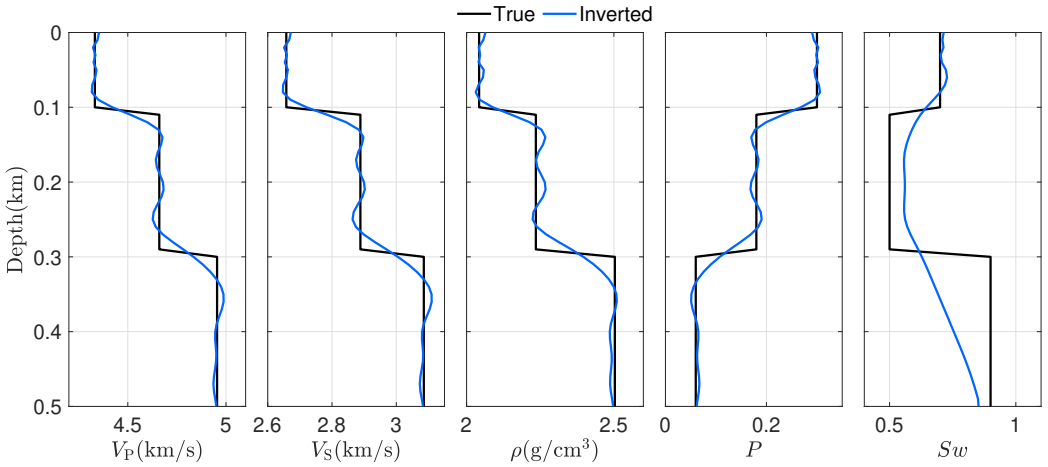

FIG. 11. Unconstrained joint inversion: model profiles at x=0.12km.

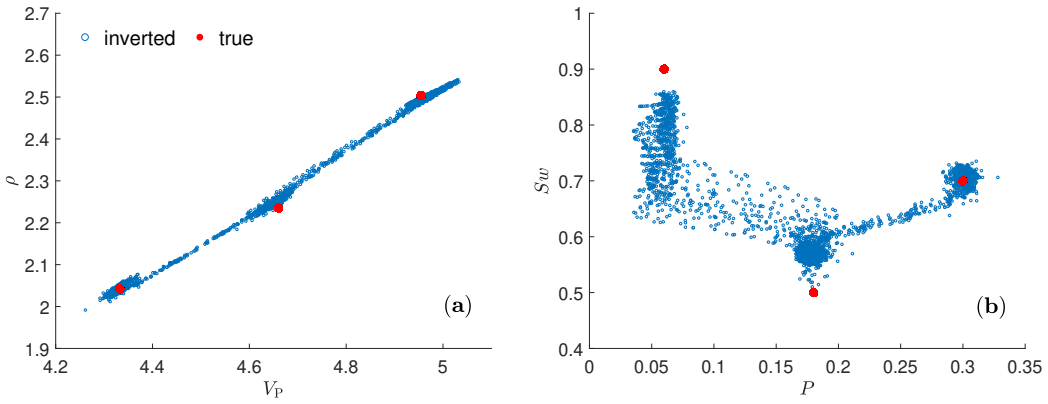

FIG. 12. Unconstrained joint inversion: crossplots.

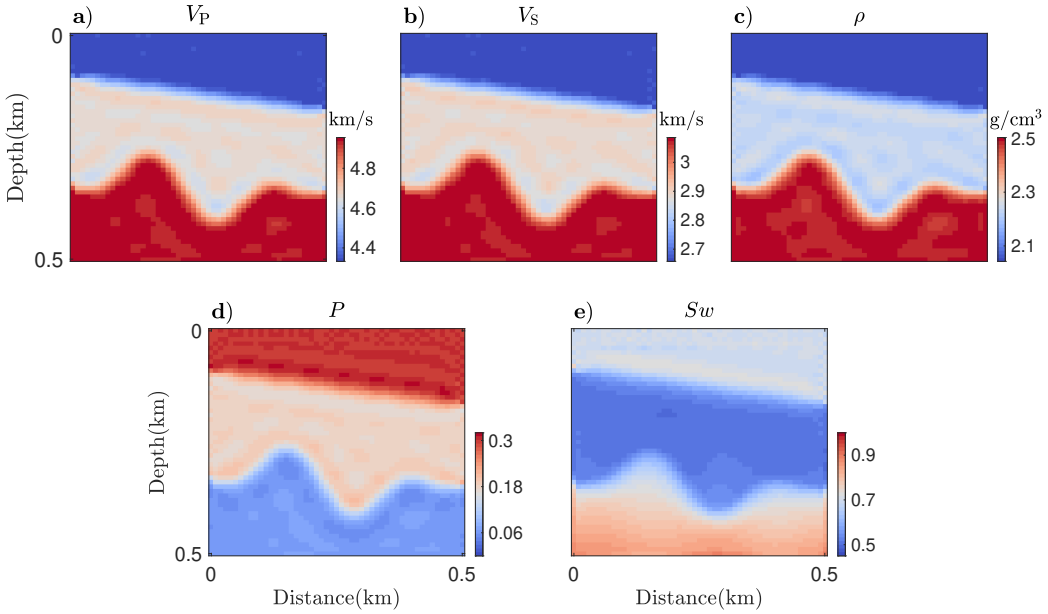

FIG. 13. Constrained joint inversion: recovered models.

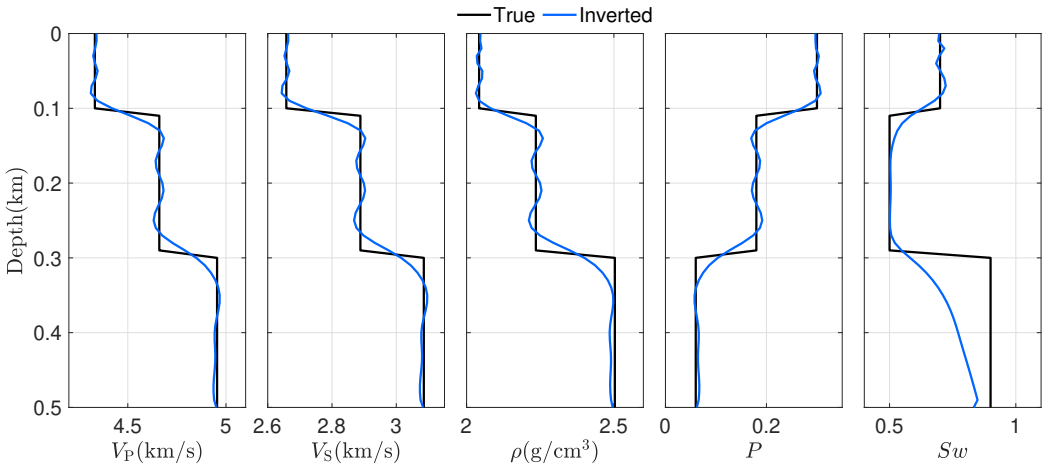

FIG. 14. Constrained joint inversion: model profiles at x=0.12km.

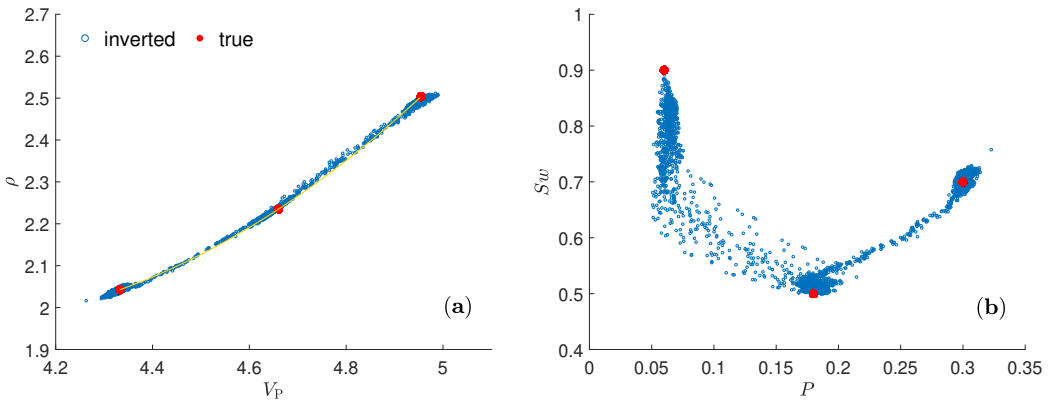

FIG. 15. Constrained joint inversion: crossplots. The yellow line denotes the V_P-ρ relation used as constraint.

Multi-facies example

Our study is based on the assumption that there is a one-to-one mapping between facies and velocity-density relation, therefore, to impose the constraint we need to predetermine the spatial distribution of facies. This step is simplified with the three-layer model, which can be well defined by a single velocity-density relation. However, it is more general that the subsurface model exhibits multiple velocity-density relations and different facies.

Here, we test the proposed method on a selected target of the Marmousi model (Figure 16). In Figure 17a we display the true models using a V_{P}-ρ crossplot. The model points (black dots) can be classified into three categories, each corresponds to a single facies / V_{P}-ρ relation. Labeling every point based on the facies it falls into, a facies map can be generated (Figure 17b). Notably, the solution of facies map is not unique. It depends on the way in which we separate those points. More groups and different fitting equations are allowed. Even the terminology "facies" we use is not strict, it is rather a tool for us to assign the correct V_{P}-ρ relation to each grid.

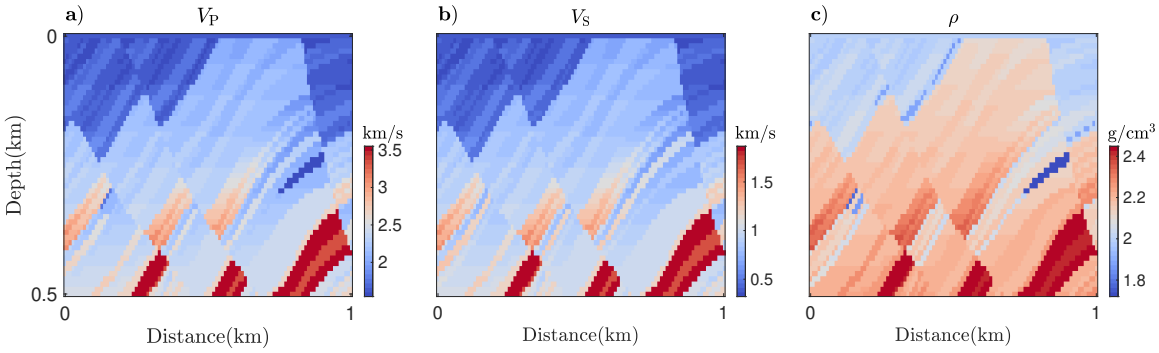

FIG. 16. Marmousi case. True models of a) P-wave velocity, b) S-wave velocity, and c) density

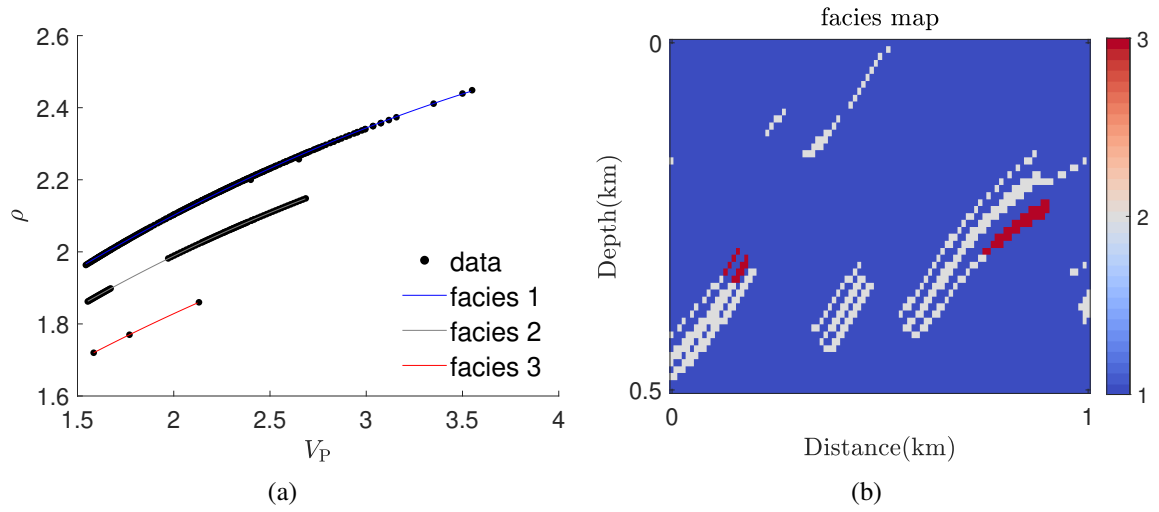

FIG. 17. Facies classification. a) Model points are classified into three groups. Fitting each group using a quadratic function: $\rho = aV_{\mathrm{P}}^2 + bV_{\mathrm{P}} + c$. b) The corresponding spatial distribution of facies.

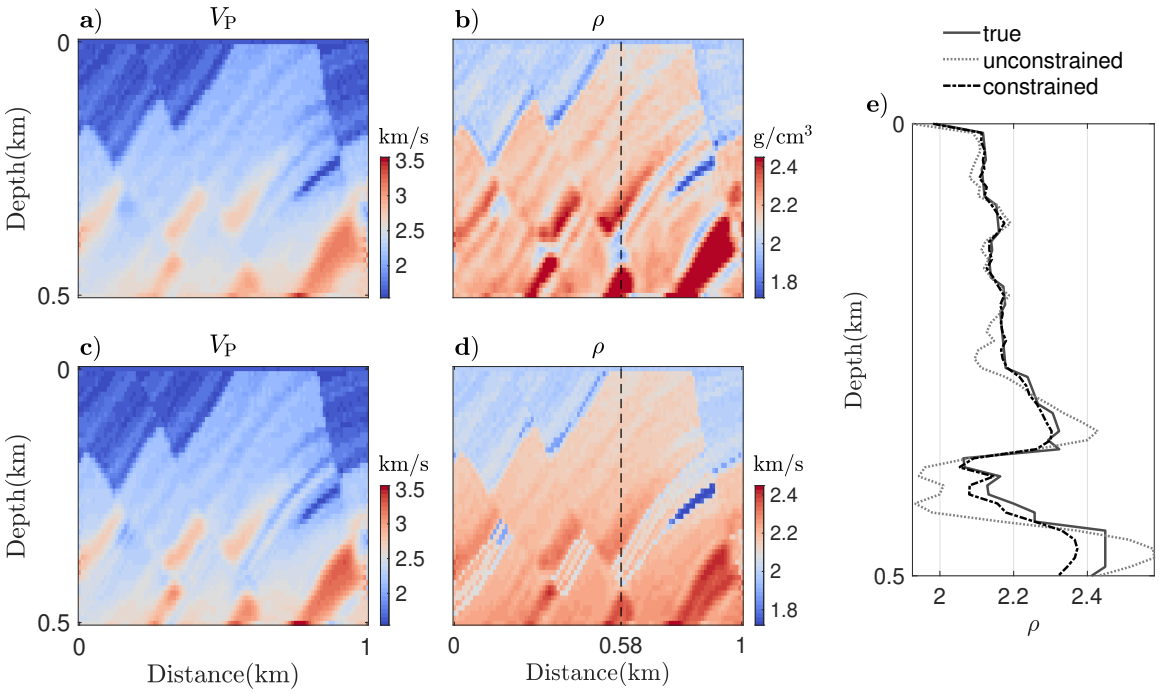

FIG. 18. Comparison between a, b) unconstrained and c, d) constrained inversion results. e) Model profiles of density at x=0.58km.

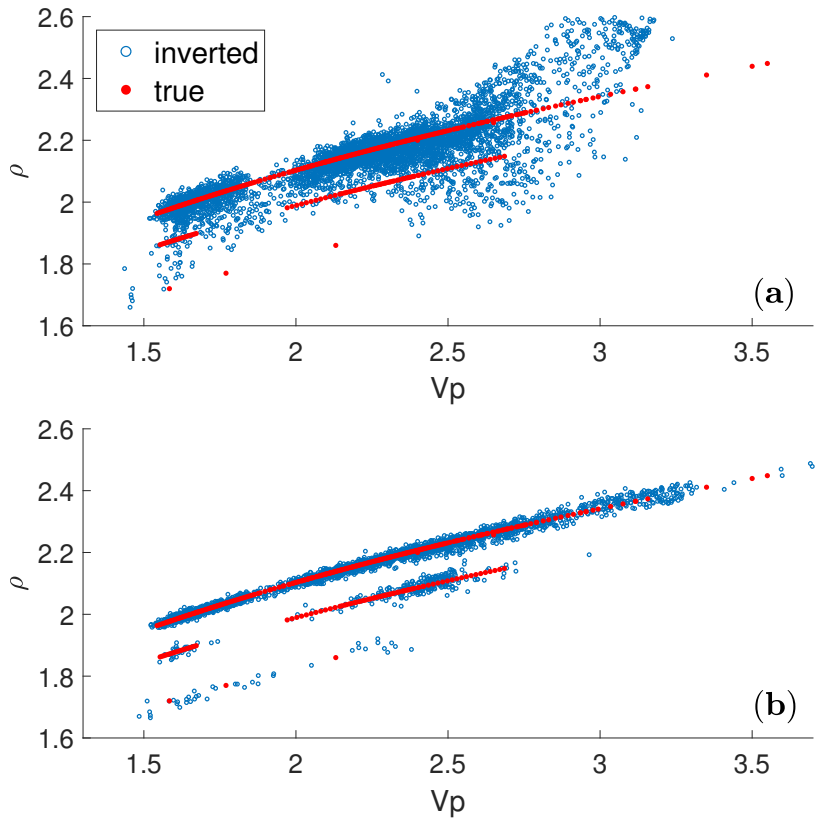

FIG. 19. Comparison between a) unconstrained and b) constrained inversion results.

However, it is unrealistic to obtain the facies map based on the true model, which is unknown. A facies classification technique is required. Some authors have proposed using an iterative approach to impose facies-based constraints (e.g., Singh et al., 2018; Zhang et al., 2018), which consists of estimating the facies distribution based on the current inverted model, and then using this facies distribution to constrain the inversion at the next iteration. By doing so the facies map is updated interactively with the model during the inversion. They ended up achieving a good estimation of both subsurface models and facies map. Unfortunately, we have not yet found this approach effective for imposing the kind of constraint we propose. Our study indicates that the iterative approach will inevitably assign the wrong facies to part of the model at each iteration, and hinder the model from updating towards reducing data misfit. As a result, it can be less efficient than the unconstrained inversion.

While our research into facies classification is ongoing, we examine the proposed method using the exact facies distribution (Figure 17b). In Figure 18 we compare the inversion results between the unconstrained and constrained approaches. The recovered density model using the constrained approach has a higher resolution (Figure 18d) and matches the true model more closely (Figure 18e). Figure 19b illustrates that the inverted model points are confined to different lines honoring their corresponding facies, thus being more likely to recover the true model points.

CONCLUSIONS

We propose a regularized EFWI scheme that includes rock physics information as a model penalty term. This term is in the form of facies-based velocity-density relations. We illustrate how it helps to constrain a sequential workflow and a joint workflow for recovering elastic and rock physics properties. Parameters such as density and water saturation that are difficult to estimate with the unconstrained inversion are better resolved using the constrained approach. The joint inversion is computationally more efficient and can guarantee the consistency between elastic and rock physics property recoveries. A robust facies classification technique is required for applying the proposed method to complex subsurface models.

ACKNOWLEDGMENTS

We thank the sponsors of CREWES for continued support. This work was funded by CREWES industrial sponsors, and NSERC (Natural Science and Engineering Research Council of Canada) through the grant CRDPJ 461179-13 and CRDPJ 543578-19. Qi Hu was also supported by the SEG/James L.Allen Scholarship.

REFERENCES

Aragao, O., and Sava, P., 2020, Elastic full-waveform inversion with probabilistic petrophysical model constraints: Geophysics, **85**, No. 2, R101–R111.

Asnaashari, A., Brossier, R., Garambois, S., Audebert, F., Thore, P., and Virieux, J., 2013, Regularized seismic full waveform inversion with prior model information: Geophysics, **78**, No. 2, R25–R36.

Brossier, R., Operto, S., and Virieux, J., 2009, Seismic imaging of complex onshore structures by 2D elastic

frequency-domain full-waveform inversion: Geophysics, **74**, No. 6, WCC105–WCC118.

Bunks, G., Saleck, F. M., Zaleski, S., and Chavent, G., 1995, Multiscale seismic waveform inversion: Geophysics, **60**, No. 5, 1457–1473.

Castagna, J., Batzle, M., Kan, T., and Backus, M., 1993, Rock physics—the link between rock properties and avo response: Offset-dependent reflectivity—Theory and practice of AVO analysis: SEG, **8**, 135–171.

Dupuy, B., Garambois, S., Asnaashari, A., Balhareth, H. M., Landrø, M., Stovas, A., and Virieux, J., 2016a, Estimation of rock physics properties from seismic attributes—part 2: Applications: Geophysics, **81**, No. 4, M55–M69.

Dupuy, B., Garambois, S., and Virieux, J., 2016b, Estimation of rock physics properties from seismic attributes—part 1: Strategy and sensitivity analysis: Geophysics, **81**, No. 3, M35–M53.

Gardner, G., Gardner, L., and Gregory, A., 1974, Formation velocity and density—the diagnostic basics for stratigraphic traps: Geophysics, **39**, No. 6, 770–780.

Geng, Y., Pan, W., and Innanen, K. A., 2018, Frequency-domain full-waveform inversion with non-linear descent directions: Geophysical Journal International, **213**, No. 2, 739–756.

Grana, D., 2016, Bayesian linearized rock-physics inversion: Geophysics, **81**, No. 6, D625–D641.

Guitton, A., 2012, Blocky regularization schemes for full-waveform inversion: Geophysical Prospecting, **60**, No. 5, 870–884.

Hu, Q., Keating, S., Innanen, K., and Chen, H., 2020, Direct elastic full-waveform inversion of rock physics properties, *in* SEG Technical Program Expanded Abstracts 2020, Society of Exploration Geophysicists, 885–889.

Kamath, N., Tsvankin, I., and Naeini, E. Z., 2017, Facies-constrained fwi: Toward application to reservoir characterization: The Leading Edge, **36**, No. 11, 924–930.

Keating, S., and Innanen, K. A., 2019, Parameter crosstalk and modeling errors in viscoacoustic seismic full-waveform inversion: Geophysics, **84**, No. 4, R641–R653.

Kuster, G. T., and Toksöz, M. N., 1974, Velocity and attenuation of seismic waves in two-phase media: Geophysics, **39**, No. 5, 587–618.

Martin, G. S., Wiley, R., and Marfurt, K. J., 2006, Marmousi2: An elastic upgrade for marmousi: The leading edge, **25**, No. 2, 156–166.

Métivier, L., Brossier, R., Operto, S., and Virieux, J., 2017, Full waveform inversion and the truncated newton method: SIAM Review, **59**, No. 1, 153–195.

Operto, S., Gholami, Y., Prieux, V., Ribodetti, A., Brossier, R., Metivier, L., and Virieux, J., 2013, A guided tour of multiparameter full-waveform inversion with multicomponent data: From theory to practice: The Leading Edge, **32**, No. 9, 1040–1054.

Pan, W. Y., Innanen, K. A., and Geng, Y., 2018, Elastic full-waveform inversion and parametrization analysis applied to walk-away vertical seismic profile data for unconventional (heavy oil) reservoir characterization: Geophysical Journal International, **213**, No. 3, 1934–1968.

Pan, W. Y., Innanen, K. A., Geng, Y., and Li, J. X., 2019, Interparameter trade-off quantification for isotropic-elastic full-waveform inversion with various model parameterizations: Geophysics, **84**, No. 2, R185–R206.

Plessix, R. E., 2006, A review of the adjoint-state method for computing the gradient of a functional with geophysical applications: Geophysical Journal International, **167**, No. 2, 495–503.

Pratt, R. G., 1990, Frequency-domain elastic wave modeling by finite differences: A tool for crosshole seismic imaging: Geophysics, **55**, No. 5, 626–632.

Rocha, D., and Sava, P., 2018, Elastic reflection waveform inversion with petrophysical model constraints, *in* SEG Technical Program Expanded Abstracts 2018, Society of Exploration Geophysicists, 1203–1207.

Sen, M. K., and Stoffa, P. L., 2013, Global optimization methods in geophysical inversion: Cambridge University Press.

Singh, S., Tsvankin, I., and Naeini, E. Z., 2018, Bayesian framework for elastic full-waveform inversion with facies information: The Leading Edge, **37**, No. 12, 924–931.

Tarantola, A., 1986, A strategy for nonlinear elastic inversion of seismic reflection data: Geophysics, **51**, No. 10, 1893–1903.

Tikhonov, A. N., and Arsenin, V. Y., 1977, Solutions of ill-posed problems: New York, 1–30.

Zhang, Z. D., Alkhalifah, T., Naeini, E. Z., and Sun, B. B., 2018, Multiparameter elastic full waveform inversion with facies-based constraints: Geophysical Journal International, **213**, No. 3, 2112–2127.